Characterization of precipitates susceptible to clogging of sump filters after a Loss-of-Coolant-Accident in PWRs

Coralie LE MAOUT ALVAREZ, Anaïs Minne, William Le Saux, Laurent Cantrel, Marie-Odile Simonnot

Characterization of precipitates susceptible to clogging of sump filters after a Loss-of-Coolant-Accident in PWRs

Coralie Le Maout Alvarez[a,b], Anaïs Minne[a], William Le Saux[a], Laurent Cantrel[a], Marie-Odile Simonnot[b*],

[a] Institut de Radioprotection et de Sûreté Nucléaire, PSN-RES, Cadarache BP 3 – 13115 Saint Paul Lez Durance, France

[b] Université de Lorraine, CNRS, LRGP, F-54000 Nancy, France

Corresponding author: marie-odile.simonnot@univ-lorraine.fr

Abstract

During a Loss Of Coolant Accident involving a primary circuit failure in a nuclear power plant, debris, generated by the impact of the steam jet, is transported to the hot liquid phase formed at the bottom of the nuclear containment. Water is recirculated after passing through filters. Chemicals are released and may precipitate on the filters, increasing the pressure drop. This paper investigates the characterization of precipitate formation in a soda/borate buffer, due to the presence of calcium, silicon, and zinc, released from mineral fibers, concrete particles, or the corrosion of metal surfaces.

Experiments run at various temperatures and chemical compositions are presented, with the objective of identifying the precipitates and determining the critical thresholds of concentration and temperature beyond which the risk of chemical clogging disappears. The experimental results are compared to those calculated with the CHESS software, intended to calculate the speciation at thermodynamic equilibrium.

The results show the formation of amorphous precipitates: silica, calcium borates, borosilicates and zinc silicate. Precipitation is temperature dependent, with the highest masses obtained between 50 and 60 °C. The comparison of experimental and calculated results indicates a good overall consistency. This work demonstrates the importance of considering chemical clogging in this context.

Keywords

LOCA; mineral fibers; calcium-silica precipitates; temperature effect; nuclear power plant; CHESS

Highlights

- Chemical effects on of sump filter clogging in LOCA situations are studied.
- The precipitates are silica, calcium borate, borosilicate and zinc silicates.
- Precipitation is influenced by temperature and is maximal around 60 °C
- Speciation calculations (CHESS) fairly predict experimental results.
- Chemical effects contribute to the clogging of PWR sumps.

1. Introduction

In the event of a Loss of Coolant Accident (LOCA), involving a break in the primary circuit of a Pressurized Water Reactor (PWR), safety systems are implemented. A boron (in the form of boric acid) water injection safety system is activated to cool the reactor core. If the accident leads to an increase in pressure and temperature in the reactor building, the containment spray system is activated. Spraying alkaline water with soda also reduces the level of molecular iodine gas (especially 131-iodine isotope) in the atmosphere due to droplet capture. Water for both functions is initially taken from the 1 600 m^3 pool treatment and cooling system tank. When the water reaches a low level, the safety injection circuits automatically switch to recirculation mode, during which they suck up the water that has fallen into the sumps located at the bottom of the reactor building. The water collected in the sumps is a mixture of ≈0.2 M boric acid and 0.06 M sodium hydroxide. The target pH is therefore approximately 8.5. The temperature of the water in the sumps may reach 130 °C for a transient time and then slowly cool to 50 °C in the post-LOCA phase.

During a LOCA, debris is produced because of the impact of the steam jet from the primary circuit initially at 155 bars in the area near the rupture. The main debris consists of thermal insulation (mineral fibers) on the piping, degradation of paint covering the inner surfaces or latent debris such as concrete dust. Some of this debris can be transported to the sump filters by water drag and/or settling. Filters are implemented to prevent debris from flowing through fuel core channels and pumps during the recirculation water phase which can last for weeks.

In the early 1990s, several incidents in boiling water reactors (Barsebäck in Sweden, Perry, and Limerick in the United States) highlighted the risk of clogging of sump filters. In particular, during the incident that affected, on July 28, 1992, the reactor #2 of the Barsebäck power plant (Pointner et al., 2005). This accident occurred following the untimely opening of a valve, releasing 200 kg of fibrous debris (heat mineral fiber insulation used to insulate piping). Part of this debris was carried into the condensation pool, causing a significant increase in the pressure drop across the filters of the emergency cooling systems after 70 min.

These different incidents have raised questions about the possible clogging of sump filters in LOCA situations for PWRs. Indeed, depending on the characteristics of the debris (size, mass, etc.), some of it

may be carried to the filters and create a debris bed, which can cause their clogging by a physical effect coupled with a chemical effect. The speculative chemical contribution may correspond to the formation of precipitates within the fibrous bed (Sandrine et al., 2008; Tregoning et al., 2009). The formation of these precipitates may result from the presence in the solution of elements released by the corrosion/dissolution of debris and metal surfaces due to oversaturation.

For French PWRs, the debris source term is made up of i) mineral fibers composed mainly of silica (SiO_2), sodium oxide (Na_2O), and calcium oxide (CaO) at 65, 16 and 8 wt.%; ii) concrete dust, in smaller amounts, of variable composition (the composition of the concrete may depend on the reactor). In our study, the concrete powder is made of 4 and 54 wt.% of SiO_2 and CaO; iii) galvanized steel metal surfaces potentially releasing zinc (Zn) after hot water leaching. The main elements dissolved from the fibers and concrete particles are silicon (Si) and calcium (Ca). Since the amount of fiber generated in this type of accident is greater than the amount of concrete dust, so a Ca/Si molar ratio of less than unity is expected.

Concerning the galvanized steel surfaces, several thousand square meters are present in the PWR reactor buildings. The corrosion rate of galvanized steels has been widely reported (Johns et al., 2003; Niyogi et al., 1982; Piippo et al., 1997). The closest to our conditions of interest are those of Piippo *et al.* (Piippo et al., 1997). Indeed, their objectives were to carry out tests under conditions as close as possible of a LOCA to study this phenomenon of corrosion of galvanized steels. According to their results, a corrosion rate of 0.045 $g.m^{-2}.h^{-1}$ is to be considered for a pH of 8.0. Under LOCA conditions for a 900 MWe PWR, the sump water is composed of boric acid and sodium hydroxide for a pH between 8.0 and 8.5, which leads to a Zn concentration of $\approx 10^{-4}$ M after 24 hours of leaching.

Thus, knowing the composition of the debris source term, and considering that the main elements transferred into solution are Ca, Si and Zn, the open question is to status to what extent precipitates are likely to form and may contribute to increase the head loss to sump screens in LOCA conditions. Therefore, this study focuses on the formation of precipitates in the presence of Si, Ca and Zn in a buffer solution containing boric acid and sodium hydroxide at pH 8.0 to 8.5 at 25 °C. According to the literature review, many precipitates can be formed. Among the potential precipitates, hydrated calcium silicates (C-S-H) are good candidates. These hydrates have already been the subject of important research works, in particular on their formation during cement hydration (Fujii and Kondo, 1981; Greenberg et al., 1960;

Taylor, 1986). The evolution of the Ca/Si molar ratio of the solid has been investigated, several phases of C-S-H have been identified: C-S-H (α) (0.66 < Ca/Si < 1), C-S-H (β) (1 < Ca/Si < 1.5) and C-S-H (λ) (Ca/Si > 1.5) (Fujii and Kondo, 1981; Grangeon et al., 2016; Greenberg et al., 1960; Grutzeck, 1999; Taylor, 1986). Under our conditions, the Ca/Si molar ratio is less than 1, *i.e.* in the C-S-H (α) domain. For this molar ratio range, the coexistence of two different phases has been reported: C-S-H (α) and silica gels (Fujii and Kondo, 1981; Greenberg et al., 1960; Taylor, 1986). Indeed, once Ca is consumed in solution, the remaining Si will involve polymerization reactions leading to the formation of oxide networks. The polymerization reactions occur in two steps: hydrolysis which creates silanol groups (Si-OH) and condensation which converts the silanol groups to siloxane bridges (Si-O-Si) which is the basic building block of the inorganic polymer chain (Aelion et al., 1950; Brinker and Scherer, 2013). Studies have also been conducted on the delay of hydration of cement and thus the formation of C-S-H. Weiler states that the use of borate ions in the cementitious medium delays the hydration process (Weiler, 1935). Bell and Coveney investigated this phenomenon using molecular scale simulation (MOPAC software) and interpreted it as the chemisorption of borate ions on silicates resulting from the dissolution of anhydrous silicates (Bell and Coveney, 1998). This phenomenon would slow down the growth of silicate chains, with the formation of borosilicate species. Other species likely to precipitate are calcium borates. Table 1 lists the different calcium borate mineral species with the reagents used, the synthesis temperatures, and the pH range according to the literature data.

Furthermore, if dissolved zinc is present, a zinc-based silicate can be formed at a relatively low temperature (20 to 104°C). This is mostly an amorphous precursor that crystallizes after calcination at ~1000°C to form willemite (Zn_2SiO_3) (Takesue et al., 2009). Finally, zinc borate precipitates are likely to be formed. Finally, precipitates of zinc borate are likely to form. Their formation is highly temperature dependent: around 25 °C they have low zinc and high boron content, while around 90 °C they are richer in zinc oxides (Kryk et al., 2014).

This brief literature review demonstrates that a wide variety of compounds are likely to be formed; under our specific conditions, experimental data are needed to characterize the nature and amount of precipitates.

This paper presents results of analytical tests devoted to study of potential chemical effects relative to sump filter clogging that can occur in a LOCA situation. The experimental results will be compared to the data from the simulations using the CHESS calculation code (De Windt and Lee, 2002). The objective is to understand and identify the nature of the precipitates and to determine the critical thresholds in terms of species concentration and temperature beyond which the risk of precipitate formation is evidenced.

Table 1 – Summary of calcium borate mineral species with reagents used synthesis temperature and pH range

Mineral species of calcium borate	Reagents	Temperature	pH range	References
Inyoite ($Ca_2B_6O_{11}.13H_2O$)	$Ca(OH)_2 + H_3BO_{3(aq)}$	-	7.4 to 9.6	(Gode, 1970; Yılmaz et al., 2012)
Gowerite ($CaB_6O_{10}.5H_2O$)	$CaCO_3 + H_3BO_{3(aq)}$	80 to 100 °C	-	(Erd et al., 1959; Yilmaz et al., 2018)
	$Ca(CH_3COO)_2 + H_3BO_{3(aq)}$	25 °C	-	
Nobleite ($CaB_6O_{10}.4H_2O$)	$CaO + H_3BO_{3(aq)}$	70 °C	-	(Erd et al., 1959)
	$Ca^{2+} + H_3BO_{3(aq)}$	-	5.5 to 7.4	(Gode, 1970)
Hexahydroborite ($CaB_2O(OH)_6.2H_2O$)	$Ca^{2+} + H_3BO_{3(aq)}$	-	9.6 to 13.6	(Gode, 1970)
Parasibirskite ($Ca_2B_2O_5.H_2O$)	$Ca(OH)_2 + H_3BO_{3(aq)}$	100 to 400 °C	-	(Hart and Brown, 1962; Lehmann et al., 1958; Liu et al., 2004; Sun et al., 2011)
Colemanite ($Ca_2B_6O_{11}.5H_2O$)	$Ca(OH)_2 + H_3BO_{3(aq)}$	100 °C	-	(Hart and Brown, 1962)

2. Materials and methods

2.1 Experimental set-up

A 1-liter solution was prepared by adding 14.3 g of boric acid (H_3BO_3, Alfa Aesar, 99%) and 60.0 mL of 1 M sodium hydroxide (NaOH, Fisher) in ultrapure water. This solution was divided into three aliquots named S1 and S2 of 490.0 mL each and S3 of 20.0 mL to make the stock solutions. Three stock solutions were prepared by adding 1) calcium chloride ($CaCl_2$, Alfa Aesar, 97%) to S1, 2) sodium silicate (Na_2SiO_3, Alfa Aesar) to S2 and 3) zinc chloride ($ZnCl_2$, Alfa Aesar, 98%) to S3. The concentration values of calcium (Ca), silicon (Si) and zinc (Zn) for each experiment are shown in Table 2 and Table 3. Three temperatures were used to study the influence of precipitation kinetics as a function of temperature (30, 60, and 90 °C).

The experiments were performed in a thermostated 1-L jacketed glass reactor. Solutions S1, S2, and S3 were successively added to the reactor, which was heated to the target temperature. The mixture was

kept homogeneous with stirring (130 rpm) using a propeller stirrer. The temperature was controlled by a thermoregulator associated with a K-type thermocouple immersed directly in the mixture, the temperature accuracy was ±2 °C. Liquid samplings were taken regularly for analysis. After 24 h, the remaining solution was filtered on a Büchner to recover any precipitates that may have formed. The precipitates were washed with a small quantity of ultrapure water (10.0 mL) to remove the species adsorbed on the surface. They were then dried in an oven at 60 °C for 12 h before weighing.

2.2 Analysis

For each sample, the pH was measured at 25 °C, then the concentrations of dissolved Ca, Si and Zn cations were measured in a 0.2 M nitric acid (HNO_3, VWR, 69%) solution using a Perkin Elmer Optima 800 DV ICP-AES.

The precipitates were characterized by different techniques. Crystallinity was examined by X-ray diffraction (XRD), using a Bruker D8 Advance A25 model XRD instrument with a Bragg-Brentano mode (θ-2θ) geometry, ranging from 3 to 50° (2θ). Morphology and structure were determined using a Zeiss Sigma 500 VP model SEM and chemical (or elemental) analysis was performed using an Oxford Isis 300 EDS system in conjunction with SEM. A Nicolet IS50 FTIR Tri-Detector Gold Spectrometer with an integrated ATR module and a monolithic diamond crystal was used in the 4000-450 cm^{-1} wave range. Both elemental and molecular surface analysis was performed using a ToF-SIMS 5 (ION-TOF) spectrometer which has an ion gun generating a beam of primary Bi^{3+} (25 KeV; 0.2pA), representing the analysis beam.

2.3 Experimental grids

A test matrix was established by varying only the concentrations of Ca ($6.2\ 10^{-4}$ to $1.9\ 10^{-3}$ M) and Si ($1.6\ 10^{-3}$ to $5.3\ 10^{-3}$ M). The temperature was set at 60 °C and the test duration at 24 h (Table 2 - grid I). To study the impact of temperature on precipitation, additional tests were carried out by varying the temperature (30 to 90°C) for the tests that produced a precipitate at 60 °C (Table 2 - grid II).

Table 2 – Test performed in H_3BO_3/NaOH solution – pH_i 8.5 (at 25 °C) – 24 hours (impact of Ca and Si concentrations and temperature)			
	Grid I - Temperature set at 60 °C		**Grid II** - Temperature variation
Test #	$[Ca^{2+}]$ (M)	$[Si^{4+}]$ (M)	Temperature (°C)
1	$6.4.10^{-4} \pm 6.4.10^{-6}$	$5.3.10^{-3} \pm 5.3.10^{-5}$	-
2	$1.2.10^{-3} \pm 1.2.10^{-5}$		-
3	$1.9.10^{-3} \pm 1.9.10^{-5}$		30, 90
4	$6.4.10^{-4} \pm 6.4.10^{-6}$	$1.1.10^{-2} \pm 1.0.10^{-4}$	-
5	$1.2.10^{-3} \pm 1.2.10^{-5}$		30, 45, 75 and 90
6	$1.9.10^{-3} \pm 1.9.10^{-5}$		30, 90
7	$6.4.10^{-4} \pm 6.4.10^{-6}$	$1.6.10^{-2} \pm 1.6.10^{-4}$	-
8	$1.2.10^{-3} \pm 1.2.10^{-5}$		30, 90
9	$1.9.10^{-3} \pm 1.9.10^{-5}$		30, 90

Finally, the study was completed by adding Zn between $0.9.10^{-4}$ to $7.7.10^{-4}$ M, this upper range was intended to better highlight some precipitation process and reduce weighing uncertainties. All the tests, where no precipitation had been observed with Ca and Si, were performed in the presence of Zn (Table 3). In addition, as a comparison, test #5 was carried out in the presence of Zn at different temperatures (30, 60, and 90 °C) (Table 3).

Table 3 – Test performed in H_3BO_3/NaOH solution – pH_i 8.5 (at 25 °C) – 24 hours (impact of the addition of a metallic additive: zinc)				
Test #	$[Ca^{2+}]$ (M)	$[Si^{4+}]$ (M)	$[Zn^{2+}]$ (M)	Temperature (°C)
1.Zn	$6.4.10^{-4} \pm 6.4.10^{-6}$	$5.3.10^{-3} \pm 5.3.10^{-5}$		60
2.Zn	$1.2.10^{-3} \pm 1.2.10^{-5}$		Between	60
4.Zn	$6.4.10^{-4} \pm 6.4.10^{-6}$	$1.1.10^{-2} \pm 1.0.10^{-4}$	$8.8.10^{-5} \pm 8.9.10^{-6}$	60
5.Zn	$1.2.10^{-3} \pm 1.2.10^{-5}$		to	30, 60, 90
7.Zn	$6.4.10^{-4} \pm 6.4.10^{-6}$	$1.6.10^{-2} \pm 1.6.10^{-4}$	$7.7.10^{-4} \pm 7.7.10^{-5}$	60
8.Zn	$1.2.10^{-3} \pm 1.2.10^{-5}$			30

2.4 Software for calculating equilibria in solution

The CHESS software allows simulating the evolution of an initial chemical system towards its thermodynamic equilibrium state (De Windt and Lee, 2002; Lartigue et al., 2020). All calculations are based on the formation constants of chemical species given in a thermodynamic database. CHESS calculates the ionic activity products and evolves the system through reactions in solution, precipitation,

or dissolution to match the formation constants entered in the database. This equilibrium calculation code does not take into account kinetic limitations. This may lead to uncertainties, as precipitation is a complex process, which may involve non-equilibrium situations.

To ensure good consistency between experimental results and simulation data, it is necessary to verify that the expected species are present in the databases. Moreover, it is important to ensure that the thermodynamic constants (log Ks) are given at the study temperatures, *i.e.* up to 90 °C. To meet all these requirements, the databases chosen were *chess.tdb* and *tdbvit0.tdb* (De Windt and Lee, 2002) which are the most complete for our study.

For each calculation, the input data were sample volume (set to 1 L), pH, temperature and species concentrations. The pH value was not fixed to check the coherence between the experimentally measured value and the one from the simulation. The concentrations of boric acid and sodium hydroxide were set at 0.23 and 0.06 M respectively. The content of carbon dioxide gas was set at a fugacity coefficient at 3.1mol.% which represents the CO_2 partial pressure in the atmosphere. The concentrations of Ca, Si and Zn, as well as temperature were input to match the conditions listed in Table 2 and Table 3.

3. Results

3.1 Precipitate masses as a function of concentration and temperature

For the experiments conducted at 60 °C in the absence of Zn (Table 2, grid I), only tests 3, 5, 6, 8, and 9 resulted in precipitate formation. Within this series, the tests differed in their Ca and Si concentrations. It can be noticed that the Ca concentration strongly influences the precipitation: indeed, for Si concentrations of $1.1.10^{-2}$ and $1.6.10^{-2}$ M, the minimal Ca concentrations necessary for precipitation were respectively $1.2.10^{-3}$ and $1.9.10^{-3}$ M. For a Si concentration of $5.3.10^{-3}$ M, the minimum Ca concentration necessary to obtain a precipitate was about the same, $1.9.10^{-3}$ M.

By varying the temperature from 30 to 90 °C (Table 2, grid II) almost all the tests gave rise to a precipitate, except test #5 at 30 and 45 °C and #8 at 30 °C, which highlights the effect of temperature. Indeed, for fixed concentrations of Ca and Si and varying only the temperature, the precipitate masses obtained were different (Fig. 1).

In the presence of Zn (Table 3), all the experiments led to the formation of precipitates, whereas for most of them this was not the case in the absence of Zn. This clearly shows the involvement of new precipitation reactions. And as before, temperature has a significant influence on precipitation (Fig. 1, trial #5.Zn). In all cases, the highest mass of precipitate was reached around 60 °C (Fig. 1).

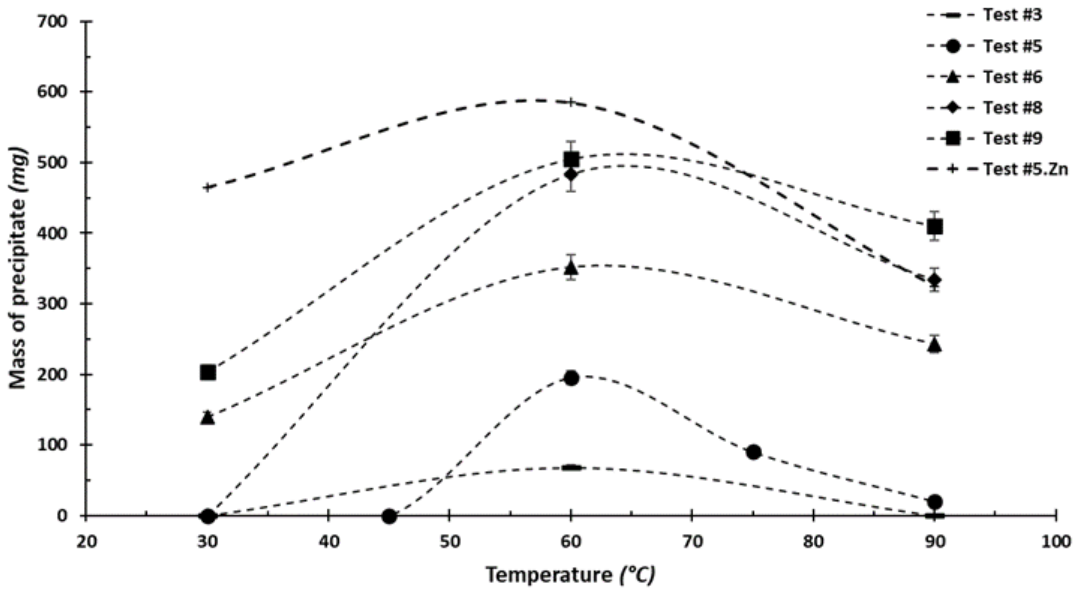

Fig. 1 – Mass of precipitate experimentally obtained as a function of temperature for fixed concentrations of Ca, Si and Zn

The addition of Zn led to a greater amount of precipitates but the temperature trend was not affected by the addition of this element. This can be explained as follows: Zn reacted very strongly to form a precipitate which, in turn, acted as a nucleus and favored the precipitation of the other precipitates determined previously.

The pH measured during the test phases was between 8.0 and 8.5 at 25 °C; this stability was due to the buffering capacity of the chemical conditioning of the solution matrix (pKa of the couple $B(OH)_3/B(OH)_4^-$ of 9.3 at 25 °C).

In Table 4 are reported the masses of Ca, Si and Zn lost in solution for test #3, 5 and 5.Zn at the different temperatures tested.

Table 4 – Mass of Ca, Si and Zn lost in solution for test #3, 5 and 5.Zn at different temperatures tested.

Test #	Temperature (°C)	Mass of Ca precipitated (mg)	Mass of Si precipitated (mg)	Mass of Zn precipitated (mg)
3	30	3.60 ± 0.36	8.37 ± 0.84	-
	60	14.0 ± 1.40	35.3 ± 3.50	-
	90	5.90 ± 0.59	14.2 ± 1.40	-
5	30	0 84 ± 0.08	2.90 ± 0.29	-
	45	0.54 ± 0.05	1.80 ± 0.18	-
	60	10.6 ± 1.60	81.6 ± 8.16	-
	75	3.21 ± 0.32	70.8 ± 7.08	-
	90	2.60 ± 0.26	45.8 ± 4.58	-
5.Zn	30	19.6 ± 2.00	113 ± 11.3	48.1 ± 4.8
	60	22.8 ± 2.38	136 ± 13.6	49.1 ± 4.9
	90	14.1 ± 1.41	123 ± 12.3	47.6 ± 4.8

For tests #3 and 5, the highest masses of precipitated Ca and Si were monitored at 60 °C; they were higher in the presence of Zn at 60 °C (Table 4); these results are in good agreement with those shown in Fig. 1. Almost the Zn present in solution was consumed, which may indicate that it was in default with respect to the stoichiometry of the reactions involved.

3.2 Characterization of the precipitates

Hereafter, only the characterization of the precipitates obtained in tests #3, 5 at 60 °C and 5.Zn at 60 and 90 °C are detailed, as the species identified are the same for all precipitates obtained in the other tests.

No diffraction peak was recorded by XRD analysis, which means that the species formed were amorphous.

Regarding the morphology of the particles, SEM imaging of precipitate #3 (Fig. 2a) revealed the presence of two different zones: one with a cluster of fine particles (Z1) and a rough zone (Z2). SEM imaging of precipitate #5 (Fig. 2b) did not show well-defined structures. EDX analysis of Z1 indicated the presence of oxygen (O) (41 wt.%), Ca (17 wt.%), and B (8.4 wt.%). The presence of these elements can be explained by the formation of calcium borate. The rough zone (Z2) contained O (55 wt.%$_s$), Si (15

wt.%), B (9.5 wt.%), and a small amount of Ca (3.1wt. %). This same result was obtained for the EDX analysis of precipitate #5 (Fig. 2b). These analyses potentially indicated the formation of silica and/or borosilicate species.

For the tests involving Zn, SEM images of the two precipitates did not show a well-defined structure. However, the 5.Zn precipitate at 90 °C (Fig. 2d) was more friable than that obtained at 60 °C (Fig. 2c). EDX analysis of Z4 location (Fig. 2c) indicated the presence of O (54 wt.%), Si (13 wt.%), and B (12 wt.%). The presence of these elements referred to the possible formation of a borosilicate species. Z5 (Fig. 2c), contained mostly O (56 wt.%) and Si (17 wt.%), which revealed the presence of silica (SiO_2). Finally, Z6 (Fig. 2d) contained mostly O (47 wt.%)), Si (33 wt.%), and Zn (8 wt.%)) which could be assimilated to zinc silicates.

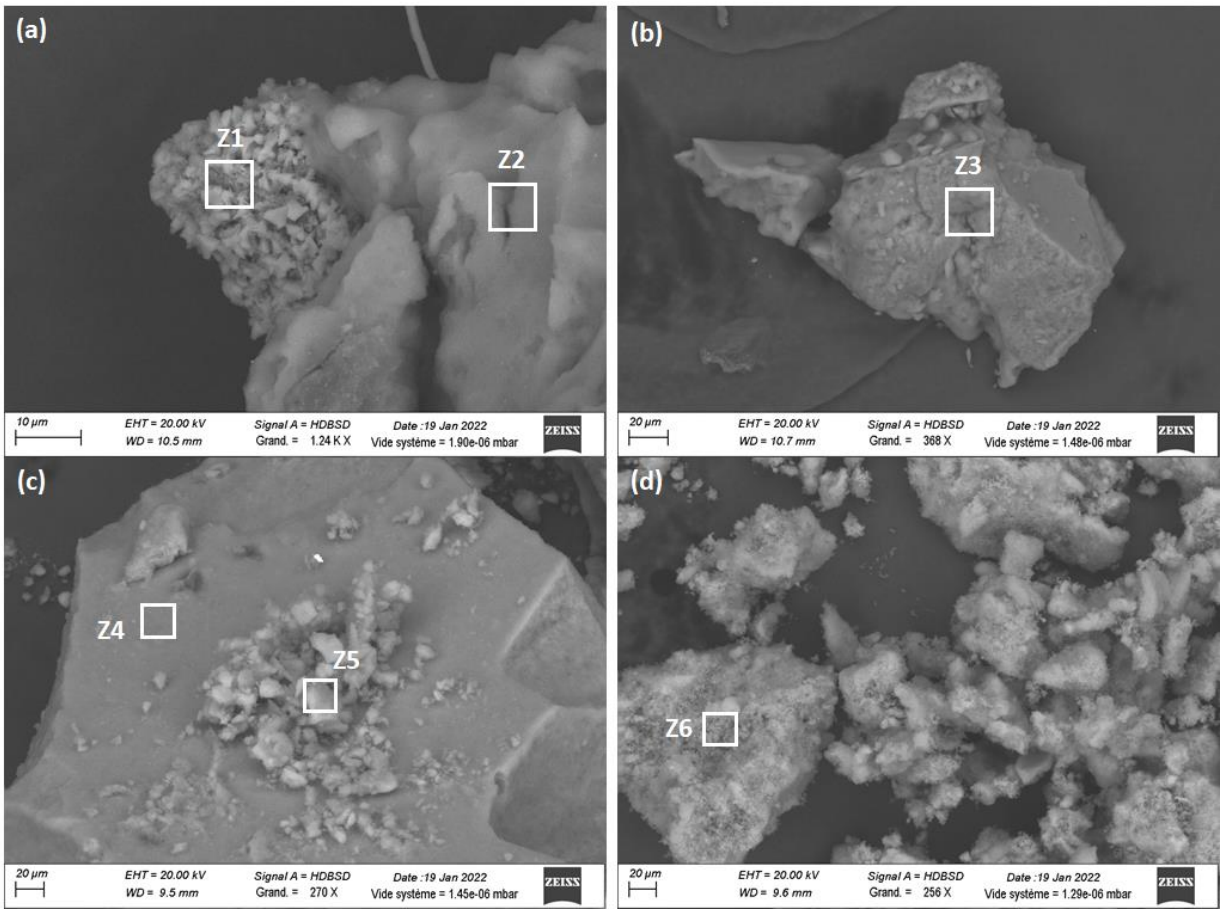

Fig. 2 – SEM images of precipitates obtained in tests #3 at 60 °C (a), #5 at 60 °C (b), #5.Zn at 60 °C (c) and 90 °C (d) with SEM-EDS analysis area

The FTIR/ATR spectra of precipitates (Fig. 3) exhibited the presence of hydroxyl groups (OH) with the elongation band ν(H-O-H) at 1 635 cm^{-1}; borate species with the elongation bands ν(B-O) at 1 409 cm^{-1} and 1 348 cm^{-1} (Kizilca & Copur, 2017; Vierne & Brunel, 1973). These bands were better defined in precipitate #3 (Fig. 3b), indeed, the initial Ca concentration of calcium in this test was higher. The bands could be attributed to the formation of calcium borate; silicate species, with the symmetrical elongation bands ν(Si-O) at 1 180 cm^{-1} and 1 045 cm^{-1} (Mollah et al., 2000); silica (SiO_2) with the elongation band ν(Si-O-Si) at 800 cm^{-1} and the deformation band δ(Si-O-Si) at 480 cm^{-1} (Mollah et al., 2000).

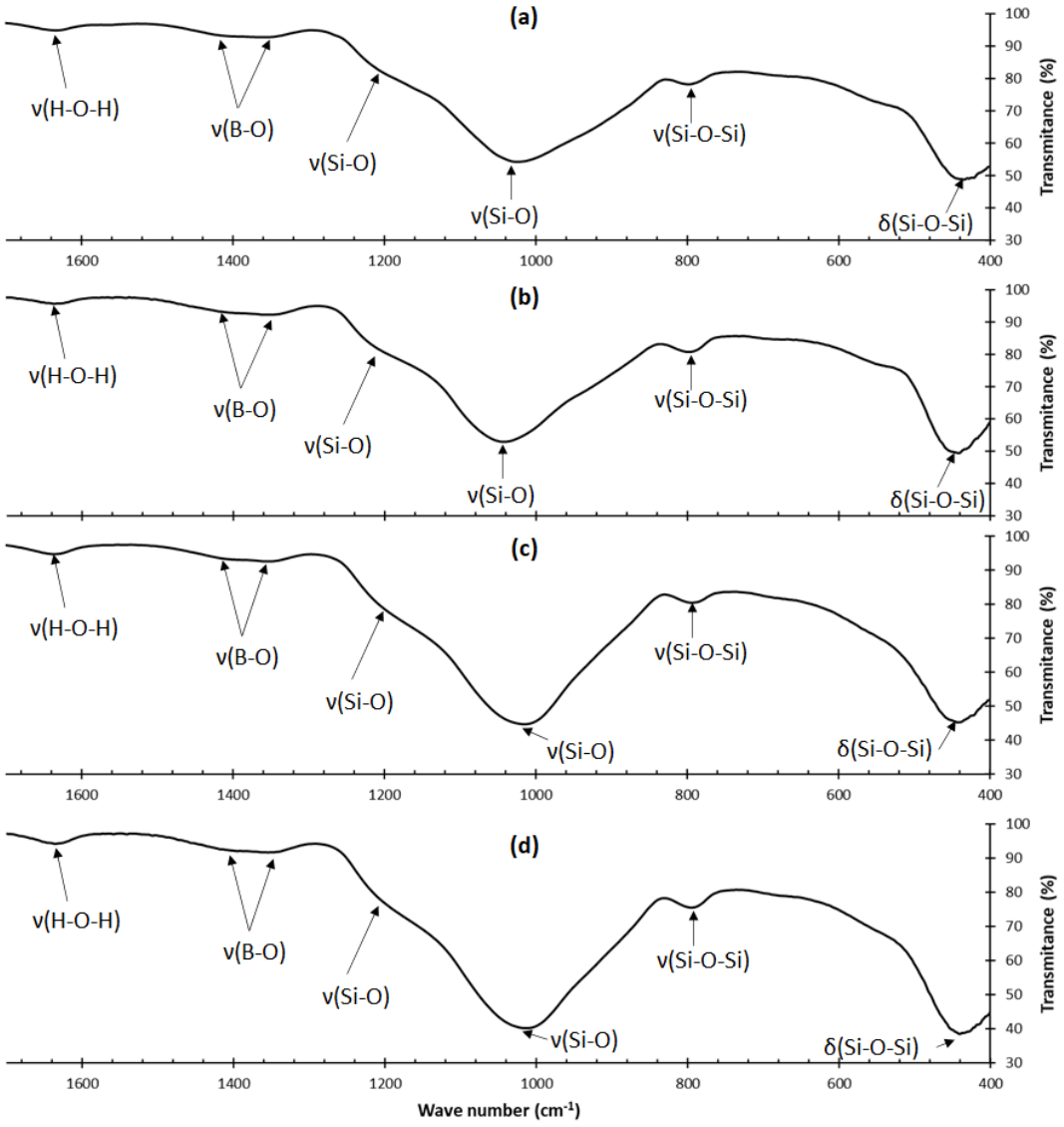

Fig. 3 – Infrared spectra of precipitates obtained in tests #3 at 60 °C(a), #5 (b) at 60 °C, #5.Zn at 60 °C (c) and 90 °C (d)

The ToF-SIMS analysis was restricted to precipitates #5 and #5.Zn at 60 °C. Table 5 list the analytical results for these two precipitates.

Table 5 – Most significant positive and negative ions intensities for precipitates #5 and #5.Zn at 60°C

Positive and negative ions	#5 at 60 °C	#5.Zn at 60 °C
Si^+	8387 ± 587.1	8643 ± 864.3
Ca^+	855.0 ± 153.9	1267 ± 76.02
$Ca_xO_yH_z^+$	368.0 ± 55.20	745.0 ± 76.02
B^+	1533 ± 137.9	782.0 ± 101.7
Zn^+	-	351.0 ± 73.71
SiO_x^-	7634 ± 305.4	5756 ± 287.8
$SiO_xH_z^-$	1693 ± 84.65	464.0 ± 41.76

Only the values of the same species (same line in the table) are comparable

Precipitate #5 at 60 °C was characterized by high intensities of silicon ions (Si^+), low mass ions characteristic of silica (SiO_x^-), high molecular weight ions corresponding to silicon (hydr)oxides or silicates ($Si_xO_yH_z^-$), boron (B^+), and a small quantity of calcium (Ca^{2+}) and its hydroxyls ($Ca_xO_yH_z^+$). Precipitate #5.Zn at 60 °C was characterized by higher intensities of Ca ions (Ca^+), their (hydr)oxides ($Ca_xO_yH_z^+$), and Si ions (Si^+). Moreover, the presence of Zn ions (Zn^+), indicates that this one reacted during the test phase. On the other hand, the intensities of low mass ions characteristic of silica (SiO_x^-), high molecular weight ions corresponding to silicon (hydr)oxides or silicates ($Si_xO_yH_z^-$), and boron ions (B^+) are lower in the presence of zinc.

These analyses confirmed the presence of silica and silicate species in both precipitates. However, the presence of Ca, B and Zn (for #5.Zn) in the precipitate indicated that they have reacted in solution but it was not possible to determine precisely the exact respective amounts of each possible precipitates, borosilicate, zinc borates, calcium borates and zinc silicates (for precipitate #5.Zn).

3.3 Simulation results

The tests presented in Tables 2 and 3 were simulated with CHESS. In the CHESS database, only one mixed calcium-boron species is present: colemanite ($Ca_2B_6O_{11}.5H_2O$).

According to the tests simulations in the Table 2, the formation of quartz (SiO_2) and colemanite ($Ca_2B_6O_{11}.5H_2O$) are predicted for each Ca and Si concentrations at temperatures ranging from 30 to 110 °C. Simulations of the tests in Table 3 additionally indicate the formation of a zinc silicate, willemite (Zn_2SiO_3) for each condition of Si, Ca and Zn concentrations at temperature ranging from 30 to 110 °C.

The influence of temperature on the precipitate mass was investigated between 30 and 110 °C for the tests #5 and #5.Zn. For both tests, the simulation indicated that the formation of quartz was favored at rater low temperature (30 °C), contrary to colemanite, whose mass formed increased from 30 to 60 °C and stabilized beyond 60 °C. In the presence of Zn, the amount of quartz formed was lower, which can be explained by the formation of willemite. On the other hand, the formation of colemanite was not affected by the presence of Zn. However, whatever the temperature, the quantity of willemite formed remained unchanged. From a general point of view, the amount of precipitate was the highest between 37 and 53 °C (Fig. 4).

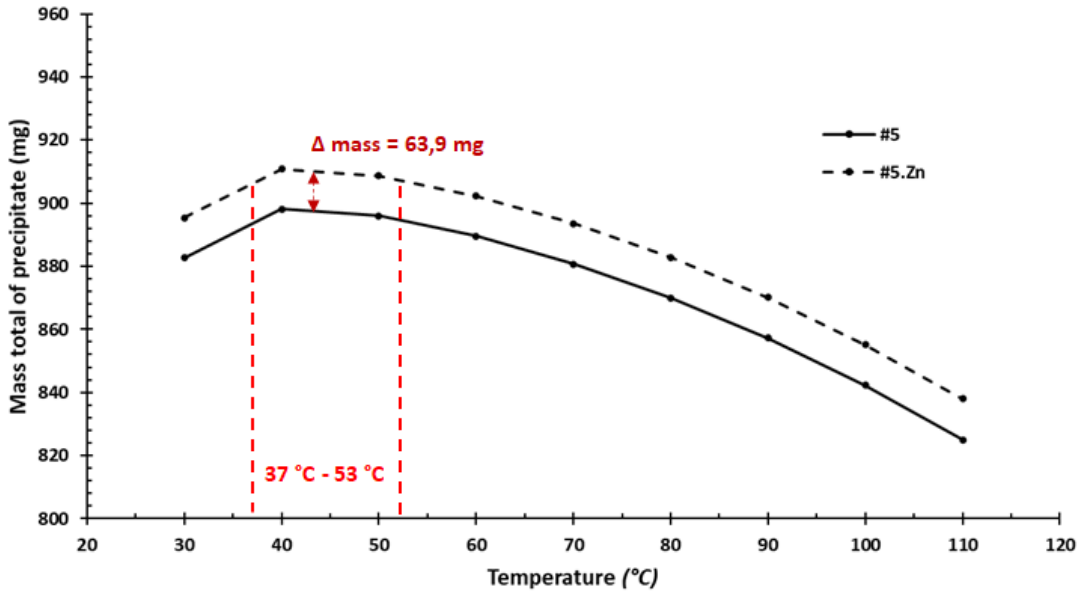

Fig. 4 – Simulation of total mass precipitation as a function of temperature for tests #5 and #5.Zn.

4. Discussion

The study of the reactivity between calcium and silicon in a solution of soda and boric acid (Table 2) showed the formation of a precipitate after 24 h under the following conditions: i) $[Ca^{2+}] \geq 1.2\ 10^{-3}$ M; $[Si^{4+}] \geq 1.1\ 10^{-2}$ M for T ≥ 60 °C; ii) $[Ca^{2+}] \geq 1.9\ 10^{-3}$ M; $[Si^{4+}] \geq 5.3\ 10^{-2}$ M for T ≥ 30 °C. The study of the impact of the addition of Zn in the system (Table 3) indicated a higher reactivity. Indeed, the

precipitation conditions were different: $[Ca^{2+}] \geq 1.2\ 10^{-3}$ M; $[Si^{4+}] \geq 1.1\ 10^{-2}$ M for T ≥ 60 °C; $[Zn^{2+}] \geq 0.9.10^{-4}$ M. The precipitate masses were the highest at approximately 60 °C and the presence of Zn did not affect the temperature dependence observed on the mass of precipitates. However, the total amount of precipitate formed was much greater in the presence of Zn.

The characterizations of the precipitates revealed the presence of amorphous species with and without Zn. Among them, the formation of amorphous silica (SiO_2) is s attested by the presence of Si-O and Si-O-Si bonds, revealed by FTIR/ATR analysis. The presence of borate species(s) was shown by FTIR with the two ν(B-O) elongation bands. Among them, the presence of calcium borate was confirmed from SEM-EDX analyses. However, several types of calcium borates exist, and their stability depends on pH. According to our pH values, the calcium borate likely to be formed is inyoite ($Ca_2B_6O_{11}.13H_2O$) due to its chemical stability between pH 7.4 and 9.6 (25 °C) (Gode, 1970; Yılmaz et al., 2012). Borosilicate has also been identified by FTIR. Indeed, borate ions can chemically bind to silicates at the end of the chain, thus blocking its propagation and the formation of calcium silicate (Bell and Coveney, 1998; Weiler, 1935). In the presence of Zn, silica, borate species and silicates were also identified. In addition, the presence of Zn inside the precipitate was identified (SEM-EDS and ToF-SIMS), but the characterization techniques did not allow to determine with certainty if this element combined with Si to form zinc silicates or boron to form zinc borates. Based on the masses consumed in the solution, the consumption of Si was greater when Zn was present, which was consistent with the assumption of a zinc silicate species. This was not observed for B, present in excess in the mixture. Nevertheless, the formation of zinc borates was strongly dependent on temperature (between 30 and 90 °C) (Kryk et al., 2014). Indeed, at low temperatures (30 °C), the zinc borates formed tended to have lower Zn and higher B content. At higher temperatures (close to 90 °C), this trend was reversed. This information may result in a low formation of this type of compound at low temperatures but was favored at higher temperatures. Experimentally, it has been shown that temperature had no impact on the formation of Zn species, so the formation of zinc borate was questioned in our test conditions.

Simulation with CHESS have indicated the formation of quartz (SiO_2), colemanite ($Ca_2B_6O_{11}.5H_2O$) and willemite (Zn_2SiO_4) for tests in the presence of Zn at the equilibrium phases. Moreover, the effect of temperature on the mass of precipitate has been demonstrated for quartz and colemanite. Indeed, the

formation of quartz is favored at the lowest temperature, and it is the opposite for colemanite. For zinc silicates, no temperature dependance was simulated.

The comparison between the experimental data and the simulations shows a rather good consistency between the identified species, except for borosilicate. Indeed, these species are absent from the database used for the simulations, and to our knowledge, no data is available in the literature to be implemented in the database. The formation of quartz indicates that the amorphous silica identified experimentally can lead to the transition from an amorphous structure to a crystalline structure in the thermodynamic equilibrium state for a more or less long period of time. Finally, for the experimentally identified calcium borate(s), the formation of inyoite can be assumed, based on its stability in the pH range of 7.4 to 9.6 and our experimental data. The simulation indicates that it is a colemanite-type calcium borate, but it is the only calcium borate formula present in the database. The crude formulas of these two species are very similar: they differ only in their degree of hydration: 5 for colemanite and 13 for inyoite thus the solubility constant should not differ a lot from one species to another. This information indicates that the calcium borate species that can be formed at thermodynamic equilibrium will have the crude formula $Ca_2B_6O_{11}.xH_2O$ with x equal to 5 or 13. Regarding the temperature effect, it was observed experimentally and by simulation. After the simulation, temperature range between 37 and 54 °C promotes the formation of a higher mass of precipitates. Experimentally, the maximum is obtained at 60 °C, knowing that the chosen temperatures were 30, 60, and 90 °C. The species formed with Zn were not formally experimentally identified, however, but data suggest the formation of zinc silicate. The simulation confirmed this hypothesis with the presence of willemite.

5. Conclusion

The objective of this work was to determine/confirm the existence of a potential chemical effect on sump filter clogging resulting from the formation of precipitates due to mineral elements released from concrete/insulation materials dissolution in solution, for different temperatures.

In the presence of Si and Ca only, effects in species concentration and temperature were observed on the reactivity of these elements. The Ca concentration mainly governs the precipitation process. On the other hand, when the system is completed by the addition of zinc under Zn^{2+} cation, this favors

precipitation whatever the temperature tested. The presence of zinc in the mixture induces new reactions which result in the formation of precipitate. Moreover, the temperature has an influence on the mass of precipitate, which is more important for a temperature close to 60 °C, this temperature where are observed the highest precipitation amounts is not affected by Zn addition. Identifications of the species formed were obtained by experimental data coupled to simulations at thermochemical equilibrium:

- Data from chemical analysis performed at the end of experiments show that the precipitates are formed by a mix of amorphous silica (SiO_2); amorphous calcium borate - possibly inyoite ($Ca_2B_6O_{11}.13H_2O$); amorphous borosilicate ($xSiO_2.yB_2O_3$); zinc - species formed not identified but potentially attributed to amorphous zinc silicates.
- Data from the simulation indicate the presence of quartz (SiO_2), colemanite ($Ca_2B_6O_{11}.5H_2O$), and willemite (Zn_2SiO_4). In the databases, borosilicate species are not listed, however, this does not exclude that the formation of this species is experimentally plausible. Moreover, an effect of temperature on mass has been demonstrated for quartz and colemanite. Indeed, the formation of quartz seems more favorable at low temperatures (30 °C); for colemanite, it is the opposite. On the other hand, for willemite, this effect is not observed. From a general point of view, according to the simulation, the quantity of precipitate formed is more important for temperatures between 37 °C and 53 °C.

From these data, chemical effects cannot be excluded and must be considered in the sump clogging issue for PWRs. The concentrations of elements (Ca, Si, Zn), as well as the critical temperatures, were determined by the formation of a precipitate in an aqueous solution containing boric acid and sodium hydroxide at pH 8.5 over 24 hours:

- $[Ca^{2+}] \geq 1.2.10^{-3}$ M; $[Si^{4+}] \geq 1.1.10^{-2}$ M; T ≥ 60 °C
- $[Ca^{2+}] \geq 1.9.10^{-3}$ M; $[Si^{4+}] \geq 5.3.10^{-3}$ M; T ≥ 30 °C
- $[Ca^{2+}] \geq 1.2.10^{-3}$ M; $[Si^{4+}] \geq 1.1.10^{-2}$ M; $[Zn^{2+}] \geq 1.5.10^{-4}$ M ; T ≥ 60 °C

Finally, the CHESS simulation tool indicates good consistency with the experimental results, although thermodynamic equilibrium is not reached under the test conditions.

Soon, this study will be completed by tests under dynamic conditions in a circulation loop. In the latter, debris will be injected into an aqueous solution composed of boric acid and sodium hydroxide pH 8.5 (at 22 °C) which can be heated up to 110 °C and circulated through a 2.5 mm steel plate filter.

To evaluate potential effect on filter pressure drop, dynamic tests should be performed to evaluate potential impact of chemical effect in relevant conditions in terms of temperature, flowrate and mass of debris.

Acknowledgements

This work was carried out at the Institut de Radioprotection et de Sûreté Nucléaire (IRSN, Cadarache) and the Laboratoire de Réaction et Génie des Procédés (LRGP, Lorraine). The authors thank IRSN for the funding. They also thank Dr Baptiste LAUBIE and Dr Bastien JALLY for the training on the CHESS simulation tool and Dr P. NERISSON for his scientific support to the writing of this article.

References

Aelion, R., Loebel, A., Eirich, F., 1950. Hydrolysis of ethyl silicate. J. Am. Chem. Soc. 72(12), 5705-5712.

Bell, I. S., Coveney, P. V., 1998. Molecular modelling of the mechanism of action of borate retarders on hydrating cements at high temperature. Mol. Simul. 20(6), 331-356. https://doi.org/10.1080/08927029808022042

Brinker, C. J., Scherer, G. W., 2013. Sol-gel science: The physics and chemistry of sol-gel processing. Academic press.

De Windt, L., Lee, J. van der., 2002. CHESS Tutorial and Cookbook (Updated for version 3.0). Ecole Nationale Supérieure des Mines de Paris, Fontainebleau, Technical Report No LHM/RD/02/13.

Erd, R. C., Mcallister, J. F., Almond, H., 1959. Gowerite, a new hydrous calcium borate, from The Death Valley Region, California. Am. Mineral. 44(9-10), 911-919.

Fujii, K., Kondo, W., 1981. Heterogeneous equilibrium of calcium silicate hydrate in water at 30 °C. J. Chem. Soc. 2, 645-651. https://doi.org/10.1039/DT9810000645

Gode, G. K., 1970. Preparation of calcium borates from aqueous solutions. Russ. J. Inorg. Chem. 15(5), 603-606.

Grangeon, S., Claret, F., Roosz, C., Sato, T., Gaboreau, S., Linard, Y., 2016. Structure of nanocrystalline calcium silicate hydrates: Insights from X-ray diffraction, synchrotron X-ray absorption and nuclear magnetic resonance. J. Appl. Crystallogr. 49(3), 771-783. https://doi.org/10.1107/S1600576716003885

Greenberg, S. A., Chang, T. N., Anderson, E., 1960. Investigation of colloidal hydrated calcium silicates. I. Solubility products. J. Phys. Chem. 64(9), 1151-1157.

Grutzeck, M., 1999. A new model for the formation of calcium silicate hydrate (CSH). Mater. Res. Innov. 3(3), 160-170. https://doi.org/10.1007/s100190050143

Hart, P. B., Brown, C. S., 1962. The synthesis of new calcium borate compounds by hydrothermal methods. J. Inorg. Nucl. Chem. 24(9), 1057-1065. https://doi.org/10.1016/0022-1902(62)80249-8

Johns, R. C., Letellier, B. C., Howe, K. J., Ghosh, A. K., 2003. Small-scale experiments: effects of chemical reactions on debris-bed head loss. NRC. NUREG/CR-6868, LA-UR-03-6415.

Kizilca, M., Copur, M., 2017. Thermal dehydration of colemanite: kinetics and mechanism determined using the master plots method. Can. Metall. Q. 56(3), 259-271. https://doi.org/10.1080/00084433.2017.1349023

Kryk, H., Hoffmann, W., Kästner, W., Alt, S., Seeliger, A., Renger, S., 2014. Zinc corrosion after loss-of-coolant accidents in pressurized water reactors – Physicochemical effects. Nucl. Eng Des. 280, 570-578. https://doi.org/10.1016/j.nucengdes.2014.09.010

Lartigue, J. E., Charrasse, B., Reile, B., Descostes, M., 2020. Aqueous inorganic uranium speciation in European stream waters from the FOREGS dataset using geochemical modelling and determination of a U bioavailability baseline. Chemosphere, 251, 126302. https://doi.org/10.1016/j.chemosphere.2020.126302

Lehmann, H.-A., Zielfelder, A., Herzog, G., 1958. Zur Chemie und konstitution borsaurer salze. I. Die hydrogenmonoborate des calciums. Z. Anorg. Allg. Chem. 296(1-6), 199-207. https://doi.org/10.1002/zaac.19582960120

Liu, Z. H., Zuo, C. F., Li, S. Y., 2004. Synthesis and thermochemistry of 2CaO·B2O3·H2O. Thermochim. Acta, 424(1), 59-62. https://doi.org/10.1016/j.tca.2004.05.029

Mollah, M. Y. A., Yu, W., Schennach, R., Cocke, D. L., 2000. A Fourier transform infrared spectroscopic investigation of the early hydration of Portland cement and the influence of sodium lignosulfonate. Cem. Concr. Res. 30(2), 267-273. https://doi.org/10.1016/S0008-8846(99)00243-4

Niyogi, K. K., Lunt, R. R., Mackenzie, J. S., 1982. Corrosion of aluminum and zinc in containment following a LOCA and potential for precipitation of corrosion products in the sump. NRC. NUREG/CP-038.

Piippo, J., Laitinen, T., Sirkiae, P, 1997. Corrosion behaviour of zinc and aluminum in simulated nuclear accident environments. STUK. STUK-YTO-TR—123.

Pointner, W., Kersting, E., Puetter, B., 2005. Generic issues on sump clogging. INIS, 37(50), 131-143.

Sandrine, R., Cantrel, L., Yves, A., Jean-Marie, M., Marek, L., Dagmar, G., Yvan, V., Bela, S., 2008. Precipitate formation contributing to sump screens clogging of a nuclear power plant during an accident. Chem. Eng. Res. Des. 86(6), 633-639. https://doi.org/10.1016/j.cherd.2008.03.016

Sun, W., Huang, Y.-X., Li, Z., Pan, Y., Mi, J.-X., 2011. Hydrothermal synthesis and single-crystal X-Ray structure refinement of three borates: Sibirskite, parasibirskite and priceite. Can. Mineral. 49(3), 823-834. https://doi.org/10.3749/canmin.49.3.823

Takesue, M., Hayashi, H., Smith, R. L., 2009. Thermal and chemical methods for producing zinc silicate (willemite): A review. Prog. Cryst. Growth Charact. Mater. 55(3), 98-124. https://doi.org/10.1016/j.pcrysgrow.2009.09.001

Taylor, H. F. W., 1986. Proposed structure for calcium silicate hydrate gel. J. Am. Ceram. Soc. 69(6), 464-467. https://doi.org/10.1111/j.1151-2916.1986.tb07446.x

Tregoning, R. T., Apps, J. A., Chen, W., Delegard, C. H., Litman, R., MacDonald, D. D., 2009. Phenomena identification and ranking table evaluation of chemical effects associated with generic safety issue 191. NRC. NUREG-1918.

Vierne, R., Brunel, R, 1973. Spectre de réflexion infrarouge de minéraux monocristallins ou en poudre III : Carbonates. Bull. Mineral. 96(1), 55-62. https://doi.org/10.3406/bulmi.1973.6779

Weiler, J. E., 1935. Method of and composition for retarding the setting time of portland cement. U.S. Patent No 2,006,426.

Yilmaz, D., Koç, N., Turan, S., 2018. Hydrothermal synthesis of calcium hexaborate pentahydrate from local boric acid and its photoluminescence characteristic. J. Aust. Ceram. Soc. 54(2), 377-382. https://doi.org/10.1007/s41779-017-0162-3

Yılmaz, A., Boncukcuoğlu, R., Bayar, S., Fil, B., Kocakerim, M., 2012. Boron removal by means of chemical precipitation with calcium hydroxide and calcium borate formation. Korean J. Chem. Eng. 29(10), 1382-1387. https://doi.org/10.1007/s11814-012-0040-1